JOURNAL OF SYNCHROTRON RADIATION

ISSN 1600-5775

Refurbishment of an Au-coated toroidal mirror by capacitively coupled RF plasma discharge

Praveen Kumar Yadav,[a,b]* Mukund Kumar,[c] Raj Kumar Gupta,[a] Mangalika Sinha,[b] J. A Chakera[c] and M. H Modi[a,b]

[a]Soft X-ray Application Laboratory, Raja Ramanna Centre for Advanced Technology, Indore, Madhya Pradesh 452013, India, [b]Homi Bhabha National Institute, Anushakti Nagar, Mumbai 400094, India, and [c]Laser Plasma Section, Raja Ramanna Centre for Advanced Technology, Indore, Madhya Pradesh 452013, India.
*Correspondence e-mail: praveenyadav@rrcat.gov.in

Received 12 July 2018
Accepted 12 March 2019

Edited by M. Yamamoto, RIKEN SPring-8 Center, Japan

Keywords: synchrotron optics; carbon contamination; RF plasma; soft X-ray reflectivity.

Deposition of synchrotron-radiation-induced carbon contamination on beamline optics causes their performance to deteriorate, especially near the carbon *K* edge. The photon flux losses due to carbon contamination have spurred researchers to search for a suitable decontamination technique to restore the optical surface and retain its performance. Several *in situ* and *ex situ* refurbishing strategies for beamline optics are still under development to solve this serious issue. In this work, the carbon contamination is removed from a large (340 mm × 60 mm) Au-coated toroidal mirror surface using a capacitively coupled low-pressure RF plasma. Before and after RF plasma cleaning, the mirror was characterized by Raman spectroscopy, soft X-ray reflectivity (SXR) and atomic force microscopy (AFM) techniques. The Raman spectra of the contaminated mirror clearly show the G (1575–1590 cm^{-1}) and D (1362–1380 cm^{-1}) bands of graphitic carbon. The SXR curve of the contaminated mirror shows a clear dip near the critical momentum transfer of carbon, indicating the presence of carbon contamination on the mirror surface. This dip disappears after removal of the contamination layer by RF plasma exposure. A decrease in the intensities of the CO bands is also observed by optical emission spectrometry during plasma exposure. The AFM and SXR results suggest that the root-mean-square (r.m.s.) roughness of the mirror surface does not increase after plasma exposure.

1. Introduction

In synchrotron radiation beamlines, Au- and Pt-coated gratings and mirrors are commonly used for monochromatization and focusing of the beam. Even under ultra-high-vacuum conditions (10^{-10} mbar or better vacuum; 1 bar = 100 000 Pa), prolonged use of these optical elements results in deposition of carbon contamination. This contamination over the optical surface takes place by dissociation and subsequent cross-linking of adsorbed hydrocarbon gases. Direct photons and secondary electrons generated on the surface of the optics both contribute to dissociations of adsorbed hydrocarbons. The relative contributions of these two mechanisms are still debatable (Boller *et al.*, 1983; Hollenshead & Klebanoff, 2006; Leontowich & Hitchcock, 2012; Yadav *et al.*, 2017). The nature (graphite-like carbon, diamond-like carbon *etc.*) and structure of the deposited carbon contamination layer depend on the residual gas pressure, photon energy and photon dose.

In our previous study, we analysed the nature of a carbon layer grown on an Au-coated toroidal mirror after prolonged use on the reflectivity beamline at the Indus-1 synchrotron source (Nandedkar *et al.*, 2002). Raman spectroscopic characterization of the deposited layer revealed that the nature of

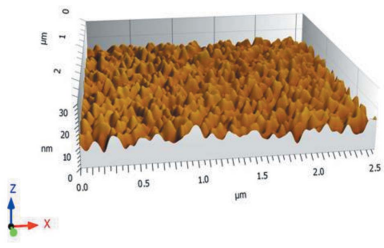

the carbon layer varies from hydrogenated tetrahedral amorphous carbon (ta-C:H) to hydrogenated graphite-like carbon (GLC:H) with photon dose along the mirror length (Yadav *et al.*, 2017). In another previous study we also concluded that the carbon layer deposited by synchrotron radiation on an LiF window not only has a graphitic nature but also has a mixed phase of carbon (carbonados) (Yadav *et al.*, 2016). Hydrogenated diamond-like carbon (DLC:H) coatings on the collector mirror of an extreme-ultraviolet (EUV) source were also observed by Dolgov *et al.* (2015).

The carbon contamination layer causes absorption near the carbon *K* edge and increases the scattered light intensity due to the increase in surface roughness caused by the deposition of carbon contamination, which leads to a decrease in the efficiency of reflection, particularly in the EUV and soft X-ray regimes. Carbon contamination on optical surfaces decreases the reflected photon flux not only near the carbon *K* edge but also at high energies. Chauvet *et al.* (2011) observed that the carbon contamination strongly affects the photon transmission after reflection at energies higher than the carbon *K* edge. For incidence angles higher than the critical angle of reflection of carbon, strong oscillations in the reflectivity *versus* photon energy curve of a contaminated mirror can be observed between 800 and 1500 eV depending on the carbon layer thickness. These oscillations are related to the interference effects of the contamination layer (Chauvet *et al.*, 2011).

Synchrotron radiation sources are especially known for their high brilliance, which is dramatically affected by contamination of the optics. To restore the photon flux in a beamline we have to refurbish or replace contaminated optics with new ones. The optics used in synchrotron radiation beamlines require high-quality coatings on premium quality substrates. These substrates and coatings can be very expensive and require a long lead time, so it is better to refurbish contaminated optics using a suitable technique. The removal of carbon contamination from beamline optical components is of special interest [especially for EUV/soft X-ray reflectivity (SXR) beamline optics] to retrieve the original optical performance. This has prompted researchers to search for and develop a suitable technique to restore the original efficiencies of contaminated optical elements. Several cleaning procedures have been suggested so far (such as DC plasma, plasma arc, laser, UV/O_3 *etc.*) but it is observed that, with these cleaning methods, either the surface is not cleaned uniformly or, in some cases, the surface is damaged or modified.

It is observed that the cleaning of graphite-like carbon (GLC) contamination, which involves a reaction with carbon and activated oxygen generated by an RF/DC plasma and photo-induction, is fairly successful in restoring the reflectivity up to the pristine level (McKinney & Takacs, 1982; Koide *et al.*, 1986, 1987). Uniformity of cleanness and surface damage can be optimized by adjusting the power feed to the plasma, the gas pressure, the exposure time and the exposure direction. In the last few years, low-pressure RF plasma glow discharge has been considered as a cost-effective, fast and very suitable method for optics cleaning. In a plasma, excited oxygen species (O*), single oxygen atoms (O) and ozone (O_3) are produced by gas discharge. These activated oxygen species react with carbon on the surface of the optics and form volatile species such as CO and CO_2 which are pumped out by dynamic pumping.

In order to test the efficiency of the RF plasma cleaning technique, Pellegrin *et al.* (2014) removed the carbon from quartz crystal, metallic foils and Au-, Rh- and Ni-coated single-crystalline Si substrates using both capacitively and inductively coupled plasma sources in conjunction with oxygen gas. They observed that the RF plasma technique is suitable for removing both graphite- and diamond-like carbon. Graham *et al.* (2002) used O_2 and H_2 RF plasmas to clean a carbon layer from an Si substrate and Mo/Si multilayer mirror. Cuxart *et al.* (2016) used an inductively coupled plasma to clean carbon contamination from large optical surfaces. They also measured the cleaning rates of carbon allotropes by varying the RF power and the distance between source and object. Pellegrin *et al.* (2014) used a capacitively coupled RF plasma system for the study of carbon cleaning rates from a quartz crystal microbalance. They observed that the carbon cleaning rate increases with increasing RF power and oxygen gas flow rate, but they did not measure the surface properties of the crystal after plasma cleaning. Recently, Moreno Fernández *et al.* (2018) used an inductively coupled RF plasma source (IBSS-GV 10X) with different combinations of feedstock gases (O_2/Ar, H_2/Ar and pure O_2) to clean B_4C-coated optics. They concluded that only a pure O_2 feedstock gas plasma exhibits the required chemical selectivity to maintain the integrity of the B_4C optical coating.

All the above-mentioned studies were performed on small samples in which carbon was intentionally deposited on small mirror samples. To the best of our knowledge, no one has used the capacitively coupled RF plasma technique to remove actual synchrotron-radiation-induced carbon contamination from a large mirror surface. In the present work, an actual synchrotron-radiation-induced carbon-contaminated gold mirror was cleaned using a capacitively coupled RF plasma system that has been developed in-house. This mirror had been used on the reflectivity beamline of the Indus-1 synchrotron source for more than a decade. The optical surface to be cleaned was placed perpendicular to the surface of the electrodes, in order to avoid damage by ion sputtering. The surface properties of the mirror before and after plasma exposure are compared here, and details of the cleaning procedure and of the retained mirror performance are discussed.

2. Experimental details

2.1. Sample for study

The sample used in the present study is a synchrotron-radiation-induced carbon-contaminated Au-coated toroidal mirror (SiO_2/Au/carbon contamination). The mirror was used as a pre-mirror (TM1) for a prolonged period of time (more than a decade) on the reflectivity beamline (BL-04) of the Indus-1 synchrotron radiation source (shown in Fig. 1). The

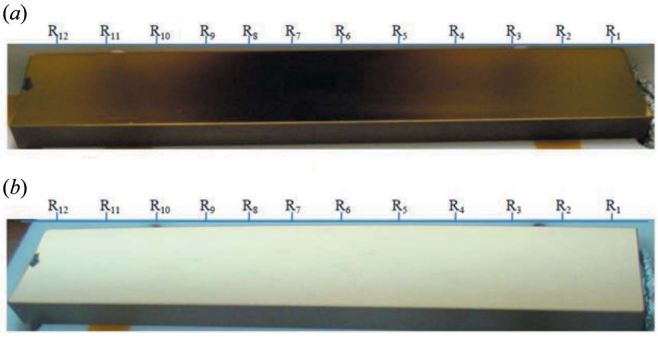

Figure 1
The Au-coated toroidal mirror used in the present work (340 × 60 × 40 mm). (*a*) The mirror before cleaning, contaminated by synchrotron-radiation-induced carbon contamination. (*b*) The mirror after cleaning using an RF plasma at 10 W for 1 h. The symbols R_1 to R_{12} indicate the points along the mirror length where the Raman spectra were measured.

mirror was exposed in the beamline to all kinds of photon energies, from infrared (IR) to soft X-rays. The mirror has dimensions of 340 × 60 × 40 mm and accepts a photon beam of 5.9 mrad (vertical) × 10 mrad (horizontal) at a 4.5° incidence angle.

The deposition of carbon takes place by dissociation of adsorbed hydrocarbon molecules on the mirror surface by direct photons and/or by secondary electrons generated at the surface of the mirror. These dissociated carbons are cross-linked and form a continuous layer on the surface of the mirror. The profile of the beam on the mirror surface is Gaussian in shape, and as a result the photon flux on the mirror surface varies along its length and has a maximum at the centre of the mirror. Because of this high photon flux at the centre of the mirror, dissociations of hydrocarbon molecules reach a maximum in the central region of the mirror. The thickness of the resulting contamination layer is thus also expected to be a maximum near the central region of the mirror. A photograph of the contaminated mirror is shown in Fig. 1(*a*).

2.2. Cleaning of carbon-contaminated mirror by capacitively coupled RF plasma

Fig. 2 shows the capacitively coupled RF plasma system developed in-house. The system consists of an assembly of aluminium electrodes (300 × 100 × 5 mm) housed inside a cylindrical vacuum chamber of diameter 450 mm and length 400 mm, an RF amplifier (operating at 13.56 MHz frequency) with an automatic tuning network (used for impedance matching or to reduce the reflected power by matching the impedance), mass flow controllers, vacuum gauges and a pumping system. The RF power was fed to the top electrode and the bottom electrode was kept at the ground potential. The electrodes are perfectly isolated from rest of the chamber and are separated from each other by ∼70 mm. In the process chamber, a base pressure of the order of 10^{-7} mbar was achieved with a turbo molecular pump. Before cleaning the actual mirror in this system, parameters such as the RF power, exposure time and process gas pressure were optimized on test samples of carbon-coated Pt thin films [Si substrate/Pt (450 Å)/C (300 Å)] prepared using DC magnetron sputtering. The samples/optics to be cleaned were positioned at the

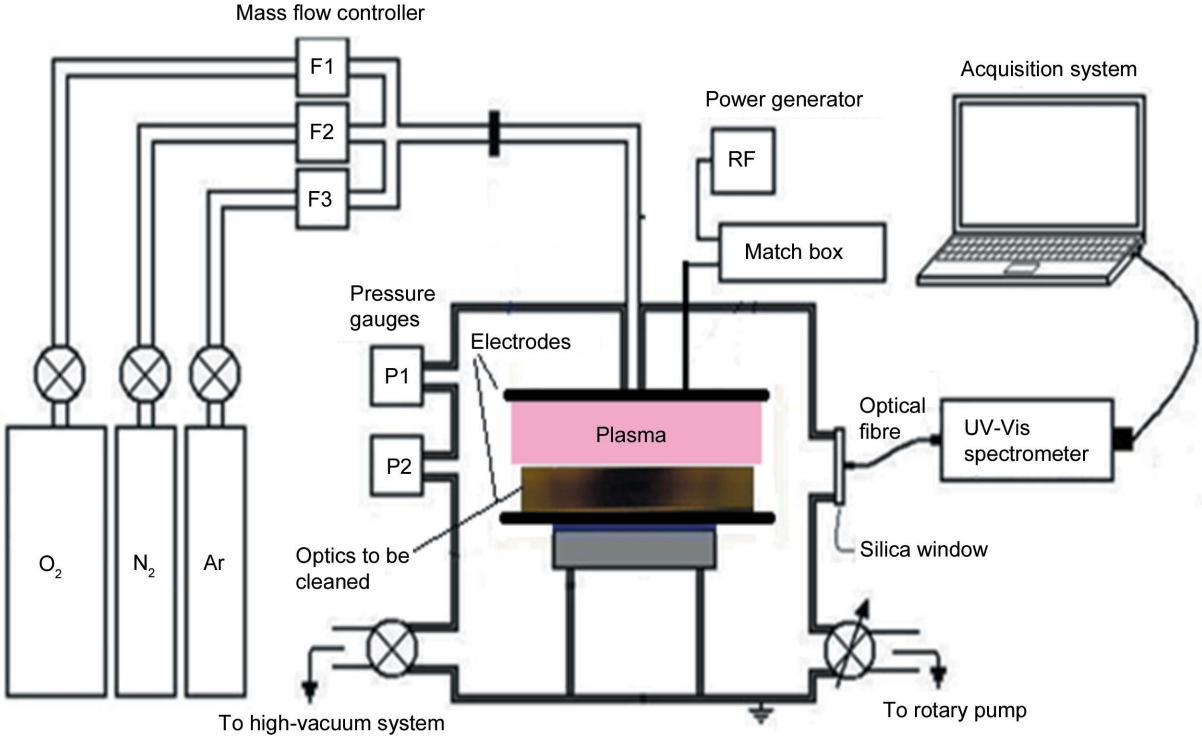

Figure 2
The RF (13.56 MHz) plasma cleaning system developed in-house. The optical surface to be cleaned was kept perpendicular to the surface of the electrodes. The dimensions of the electrodes are 300 × 100 × 5 mm. Ar and O_2 were used as feedstock gases for plasma generation.

bottom electrode, keeping the contaminated surface perpendicular to the surface of the electrodes in order to avoid a direct hit of energetic ions on the reflecting surface, which may damage or increase the roughness of the reflecting surface. During plasma exposure, the flow rates of the oxygen and argon gases were maintained at 20 sccm each in order to maintain a pressure of 3–5 $\times$ 10^{-2} mbar in the process chamber.

During optimization, it was observed that at an RF power of 10 W (33.3 mW cm^{-2}), a gas pressure of 5 $\times$ 10^{-2} mbar in the process chamber was suitable for removing the 300 Å carbon layer in 30 min without affecting the roughness of the surface. Wang *et al.* (2012) also observed similar optimized parameters while studying the effect of RF plasma cleaning on a GaAs substrate by varying the RF power, gas pressure and gas flow rate. They observed that GaAs samples treated at an RF power of 8 W, with a gas pressure in the process chamber of 4.7 $\times$ 10^{-2} mbar, an Ar flow rate of 40 sccm and a cleaning time of about 48 min, were free from damage.

In order to clean the actual contaminated mirror it was also placed on the bottom electrode, keeping the contaminated surface perpendicular to the electrode surface, and the optimized parameters (RF power 10 W, process pressure 5 $\times$ 10^{-2} mbar and exposure time 1 h) were used for the exposure. The optical spectra of the molecular bands of carbon monoxide (CO), carbon dioxide (CO_2) and oxygen (O) were simultaneously monitored and recorded using a visible spectrometer (Make Avantes Inc.) during plasma exposure. The optical emission spectroscopy (OES) technique relies on monitoring the spectral-line intensity of a plasma without applying any external perturbation to it. The total time taken for carbon removal from the contaminated mirror was adjudged by the spectral intensities of the CO and CO_2 lines/bands. It was observed that the time optimized for removal of 300 Å of carbon was not sufficient to clean the mirror, so we increased the exposure time from 30 min to 1 h.

2.3. Characterization

2.3.1. Soft X-ray reflectivity (SXR). X-ray reflectivity is a sensitive tool for the characterization of thin films and multilayer structures. Film thickness, surface/interface roughness and material density can be accurately probed by this technique. Before and after plasma exposure, the structural (thickness and roughness) and optical (optical constants) parameters of the Au and C layers were measured by SXR measurements on the Indus-2 reflectivity beamline (BL-03). The details of the beamline have been published elsewhere (Modi *et al.*, 2019). Angle-dependent reflectivity measurements were performed near to the centre of the mirror (the location of maximum contamination) using 1200 eV photon energy, with the angle of incidence varying from 0 to 10° with a step size of 0.05°. The specular reflected intensity (shown in Fig. 3) was recorded by an Si photodiode detector. The angle-dependent reflectivity spectra were fitted using the Parratt formalism (Parratt, 1954). Measured and fitted reflected intensity *versus* momentum transfer ($Q_z = 4\pi\sin\theta/\lambda$) spectra

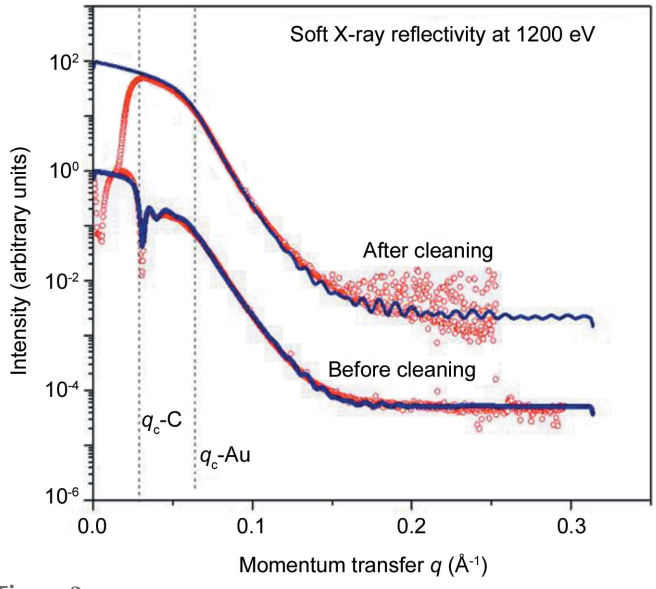

Figure 3
Measured (open circles) and fitted (continuous lines) SXR data taken before and after cleaning of the contaminated mirror using 1200 eV photon energy. Vertical dashed lines indicate the critical momentum transfers (q_c) for carbon and gold.

are shown in Fig. 3. To see the gain in the reflectivity of the mirror after plasma cleaning, the energy-dependent reflectivity in the energy range 750–1500 eV at an incidence angle of 2 $\pm$ 0.1° was measured before and after plasma cleaning. The measured reflectivity curves and fractional change in reflectivity after cleaning are shown in Fig. 4.

2.3.2. Raman spectroscopy (RS). The Raman spectra (shown in Fig. 5) from the mirror surface before and after RF plasma cleaning were recorded at room temperature with an Alpha 300SR spectrometer (Witec Instruments GmbH, Germany) using the λ = 441.6 nm line of an He–Cd laser as the excitation source. The laser light was coupled to a single-mode fibre to deliver the light to the microscope. The Raman signal was collected using a 50$\times$ (0.55 NA) microscope objective and coupled to a 100 µm (0.11 NA) multimode optical fibre, which was in turn coupled to an Action 2500i spectrometer (Princeton Instruments, USA). Twelve Raman spectra (R-1 to R-12) at 25 mm intervals along the mirror length were acquired using a TE-cooled (201 K) CCD area detector (ANDOR 420BR DD) in the spectral region of 900 to 2300 cm^{-1} at 4 cm^{-1} resolution. The spot size of the laser beam on the sample surface was about 2 µm. A low input power ($\leq$5 mW) was used to avoid any heating damage on the sample surface.

2.3.3. Atomic force microscopy (AFM). To obtain quantitative roughness measurements (before and after plasma cleaning), AFM measurements in non-contact mode were taken using a Keysight 5600LS AFM machine. In non-contact mode the surface topography is measured by sensing the van der Waals attractive forces between the tip and the surface. For surface profile comparison, three-dimensional AFM topographical images of the mirror surface, before and after plasma treatment, were taken at nearly the same location

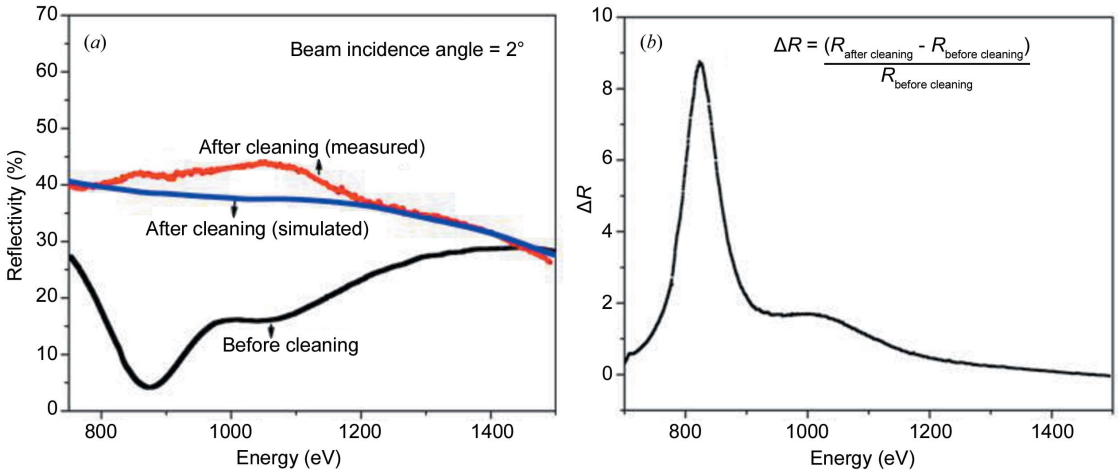

Figure 4
(*a*) Energy-dependent SXR spectra (750 to 1500 eV) of the mirror before and after RF plasma cleaning at a 2° incidence angle. (*b*) The fractional change (ΔR) in SXR after plasma cleaning.

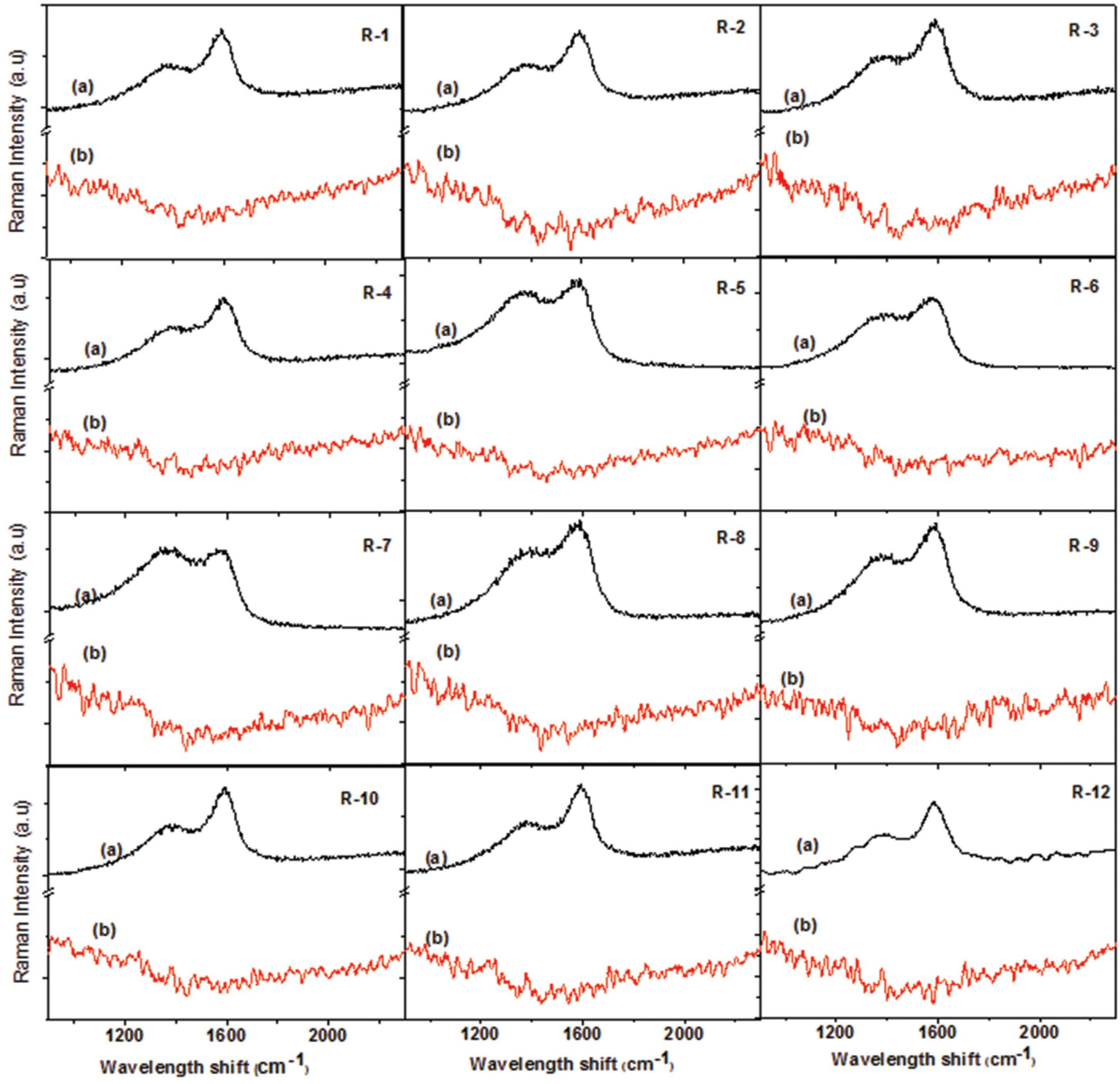

Figure 5
Raman spectra R-1 to R-12 from the mirror surface at intervals of 25 mm along the length of the mirror. Spectrum R-1 is from one edge of the mirror, R-7 from the centre of the mirror and R-12 from the opposite edge of the mirror (see positions R_1 to R_{12} in Fig. 1). In each case, the curve labelled (*a*) (black) is from the contaminated mirror surface and that labelled (*b*) (red) is after RF plasma cleaning of the mirror surface.

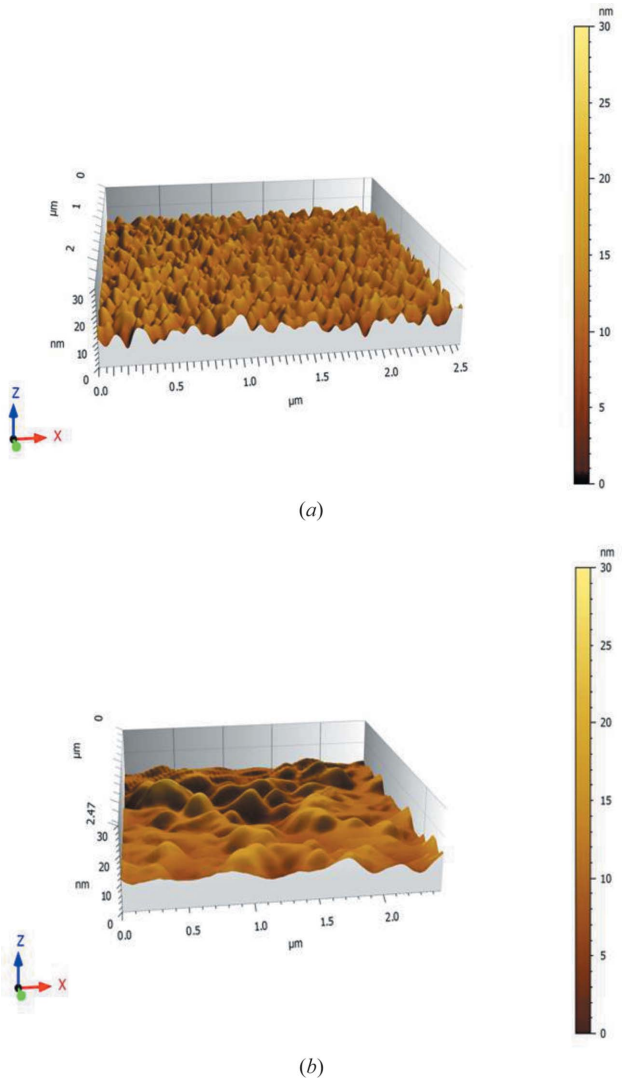

Figure 6
3D AFM images, (*a*) before cleaning the mirror and (*b*) after cleaning the mirror. The images clearly show that the surface profile changes after plasma cleaning.

under ambient conditions. Images of the mirror surface before and after plasma cleaning are shown in Fig. 6. A slight change in surface topography of the mirror is observed after plasma exposure. A decrease in the root-mean-square (r.m.s.) roughness of the mirror surface from 28 Å (the roughness of the carbon-contaminated region) to 24 Å is observed after plasma cleaning.

3. Results and discussion

We have successfully cleaned a synchrotron-radiation-induced carbon-contaminated Au-coated mirror by exposing the mirror in an RF plasma of a mixture of oxygen and argon gases. The contaminated mirror was exposed to plasma for 1 h under pre-optimized conditions (10 W RF power, 3–5 $\times$ 10^{-2} mbar pressure of oxygen and argon gas mixture) to remove carbon contamination. The carbon on the mirror surface is removed by breaking the carbon bonds (C—C, C═C, C—H, C—O *etc.*) with the synergetic effect of electrons and ions produced by UV light in the plasma. The activated carbon atoms react with oxygen radicals to form volatile gaseous species such as CO, CO_2 and hydrocarbon gases. These gaseous species are pumped out using a vacuum pumping system.

Kim *et al.* (2003) observed particle aggregations on a metal surface during cleaning with an atmospheric pressure plasma jet (APPJ). Generally, it has been observed that the surface roughness is increased by the APPJ cleaning method, and there are two possible reasons for this. The first is redeposition (particle aggregations) of removed particles onto the cleaned surface and the second is sputtering of the coating material by direct hitting of ions. In order to avoid any increase in surface roughness by ion sputtering, in our system, the RF electrode dimensions are kept the same and the electrodes are also isolated from the rest of the chamber. In such a configuration, the floating potential between the electrodes lies in the range 10–20 V and the resultant ions/electrons gain energy in the range 10–20 eV. The sputtering threshold for most metals is about 30 eV or higher. Therefore, this floating potential (10—20 V) is too low to accelerate the ions/electrons from the plasma to initiate sputtering (Belkind & Gershman, 2008).

In addition to the isolated electrode assembly, the system was also provided with a dynamic pumping mechanism that removes particles and thus avoids particle aggregations on the mirror surface. Direct ion hitting was also avoided by keeping the mirror surface perpendicular to the electrode surfaces. Different surface analysis techniques were used to characterize the mirror surface before and after plasma cleaning.

Fig. 3 shows the measured and fitted SXR curves of the toroidal mirror before and after RF plasma cleaning. The dashed vertical lines indicate the critical momentum transfers q_c-C and q_c-Au of carbon and gold, respectively. A clear dip before the critical momentum of gold (q_c-Au) in the reflectivity pattern of the contaminated mirror indicates the presence of a carbon-contaminated layer. The optical (optical constants δ and β) and structural (thickness and roughness) parameters of this contamination layer were estimated from data fitting of the reflectivity curves, while optical constants (δ and β) for graphitic carbon (GC), Au, Cr and SiO_2 were taken from the Henke tabulated database (Henke *et al.*, 1993).

During the data-fitting process, the thickness, roughness and optical constants of the carbon layer, and the thickness and roughness of the Au and Cr layers, were kept as variable parameters, while the optical constant values for Au, Cr and SiO_2 were kept as constant parameters. For data fitting after cleaning the mirror, the optical constants, thickness and roughness of GC and Au were kept as variable parameters, whereas those for Cr and SiO_2 were kept constant.

For the best fit to the reflectivity curve of the carbon-contaminated mirror, the values of the optical constants $\delta(\omega)$ and $\beta(\omega)$ of the carbon layer were estimated as 2.57×10^{-4} and 2.86×10^{-5}, respectively, and the thickness and roughness were estimated as 390 and 40 Å, respectively. The density of the carbon layer was estimated at about 75% of the density of graphitic carbon from the $\delta(\omega)$ value of carbon layer. The

Table 1
Structural parameters [thickness (t), roughness (σ)] and optical constants (δ and β) of the carbon, gold and chromium layers of the carbon-contaminated mirror before and after plasma cleaning, as obtained by fitting SXR data (1200 eV).

Element	Before cleaning				After RF plasma cleaning			
	t (Å)	δ	β	σ (Å)	t (Å)	δ	β	σ (Å)
C	390	2.57×10^{-4}	2.86×10^{-5}	40	9.5	2.01×10^{-4}	1.86×10^{-5}	4.5
Au	500	1.36 × 10−3†	5.45×10^{-4}†	16	500	1.36×10^{-3}	5.45×10^{-4}	17
Cr	90	9.32×10^{-4}†	2.73×10^{-4}†	5	90	9.32×10^{-4}†	2.73×10^{-4}†	5
Substrate(SiO_2)	Bulk	3.09×10^{-4}†	3.54×10^{-5}†	5	Bulk	3.09×10^{-4}†	3.54×10^{-5}†	5

† These values for different materials were kept constant during data fitting.

density of a material is directly proportional to the dispersive part of the refractive index [$\delta(\omega) = (n_a r_e \lambda^2/2\pi) f_1(\omega)$], where n_a is the electron density, r_e is the classical electron radius, λ is the incident wavelength and $f_1(\omega)$ is the real part of the energy-dependent atomic structure factor (Attwood, 1999).

The best fit to the reflectivity curve after plasma cleaning shows a thin low-density layer of thickness about 9.5 Å with surface roughness 4.5 Å. The optical constant values for this thin layer do not match the carbon optical constants and the Raman spectra also show an absence of carbon on the mirror surface. These observations indicate that this thin low-density layer on the mirror surface may be due to adsorption of ambient atmospheric gases. It is generally observed that, after plasma exposure, the nature of a surface becomes hydrophilic (Chou *et al.*, 2017).

The Au-layer surface roughness was estimated at 17 Å, which is nearly equal to the original estimated value for the Au layer before cleaning. The best-fit values for thickness, roughness and optical constants are given in Table 1. The tabulated values of surface roughness of the mirror surface after contamination increase from 16 to 40 Å. For comparison, after carbon contamination an increase in mirror surface roughness from 18 to 35 Å was observed on the TEMPO beamline at the SOLEIL synchrotron (a soft X-ray beamline dedicated to time-dependent photoelectron spectroscopy experiments; Chauvet *et al.*, 2011).

Koide *et al.* (1988) also observed a clear dip due to carbon in the energy-dependent reflectivity curve of a carbon-contaminated Pt-coated mirror near the carbon K edge. After cleaning by oxygen plasma at a power of 39 W and an exposure time of 50 min, they also observed a significant reduction in this carbon dip in the reflectivity curve. After cleaning, they observed that the efficiency of the mirror had increased by more than one order of magnitude in the 100–1000 eV energy range. In the present case, the energy-dependent reflectivity pattern of the contaminated mirror clearly shows two minima around 825 and 1000 eV [shown in Fig. 4(*a*)]. These minima are due to destructive interference in the carbon contamination layer. The positions of the minima on the energy scale depend on the incidence angle and the carbon layer thickness. For a fixed incidence angle, the positions of the minima shift towards higher energy as the thickness of the carbon layer decreases. After cleaning the mirror, the reflectivity losses at 825 and 1000 eV disappear, indicating that after plasma exposure the carbon layer has been removed from the surface of the mirror. The fractional change in reflectivity, $\Delta R = (R_{\text{after cleaning}} - R_{\text{before cleaning}})/R_{\text{before cleaning}}$, is plotted in Fig. 4(*b*) and it is observed that the maximum change in reflectivity occurs at 825 eV.

The soft X-ray reflectivity of the plane gold mirror was simulated at a 2° incidence angle in the 750–1500 eV energy range with a LABVIEW-based program (Modi *et al.*, 2008). For the simulation, optical constants and structural parameters are taken from Table 1. Because of the curvature in the mirror surface, the simulated reflectivity did not perfectly match with the measured reflectivity. Close matching of the simulated and measured reflectivity occurs at slightly higher incidence angle and surface roughness of the mirror, but the variation in incidence angle and roughness are within the uncertainty limits of the reflectivity measurements. The simulated and measured reflectivities are shown in Fig. 4(*a*).

Fig. 5 shows the Raman spectra (900–2300 cm^{-1} with a resolution of 4 cm^{-1}) before and after cleaning the mirror. These spectra were recorded from 12 different regions of the mirror surface (R_1 to R_{12}, shown in Fig. 1). We discussed in the *Experimental* section that the mirror in the beamline faces differing photon flux due to the Gaussian beam shape, with the result that the properties of the carbon deposited along the mirror length also vary: in the central region (R_7) the carbon layer is more graphite-like (GLC:H), while in the off-centre regions (R_1 and R_{12}) it is more like hydrogenated amorphous carbon (a-C:H) (Yadav *et al.*, 2017). The Raman spectra of the contaminated mirror clearly show the 'G' (1575–1590 cm^{-1}) and 'D' (1362–1380 cm^{-1}) Raman bands of graphitic carbon. These bands are generally present in all polyaromatic hydrocarbons. The notation arises from the Raman spectra of nanocrystalline graphite, which generally show two peaks. The D mode at about 1360 cm^{-1} is due to the A_{1g} symmetry mode at the K point. The D-mode is caused by the disordered structure of graphene: the presence of disorder in sp^2-hybridized carbon systems results in resonance Raman spectra, and thus makes Raman spectroscopy one of the most sensitive techniques to characterize disorder in sp^2 carbon materials. This mode is forbidden in perfect graphite and only becomes active in the presence of disorder (Tuinstra & Koenig, 1970). The G mode at about 1580 cm^{-1} is due to the E_{2g} symmetry mode at the Γ-point. The G-band arises from stretching of the C—C bonds (sp^2) in graphitic materials, and is common to all sp^2 carbon systems whether they are arranged in rings or chains; this mode does not require the presence of six-membered rings. In

the Raman spectra of the plasma-cleaned mirror, both G and D bands are completely absent, indicating that after plasma exposure the carbon contamination is totally removed from the surface of the mirror.

Figs. 6(*a*) and 6(*b*) show three-dimensional AFM images (2.5 × 2.5 µm) taken from the dense contaminated region before and after cleaning the mirror, respectively. The images clearly indicate that the surface topography of the mirror is changed after plasma cleaning, indicating that, when a contamination layer grows on a mirror surface by synchrotron radiation induction, the mirror surface roughness increases. An increase in surface roughness after contamination deposition was also observed by Chauvet *et al.* (2011). After removing the carbon layer from the mirror surface, the AFM and SXR measurements clearly show a decrease in surface roughness from 28 to 24 Å and 40 to 17 Å, respectively. The difference between the roughness values obtained by these two different techniques may be due to different area averaging covered by the two different measuring probes. Berman & Krim (2012) studied the effect of argon and oxygen plasma exposure on the surface roughness of an Au film. They concluded that, for equal exposure times, argon plasma bombardment produces a greater change in surface roughness and a greater material removal rate.

During plasma exposure, removal of the carbon layer from the surface of the toroidal mirror was also observed by optical emission spectroscopy (OES). The optical emission spectra (intensity *versus* wavelength) are shown in Fig. 7. The concentration of any species can be monitored by observing the intensity of the corresponding line emission. The line intensity of the recorded spectrum is proportional to the density of species in the plasma. Thus, any change in line intensity qualitatively indicates a change in the density of a particular species. We observed a change in the line intensity of two well known bands of carbon monoxide (CO) called the third positive band and the ångström band, also known as the second positive band. The wavelength span of the third positive band (transition from $b3\Sigma+$ to $a3\Pi$) is from 260 to 380 nm, whereas the wavelength span of the ångström band (transition from $B1\Sigma+$ to $A1\Pi$) is from 410 to 660 nm.

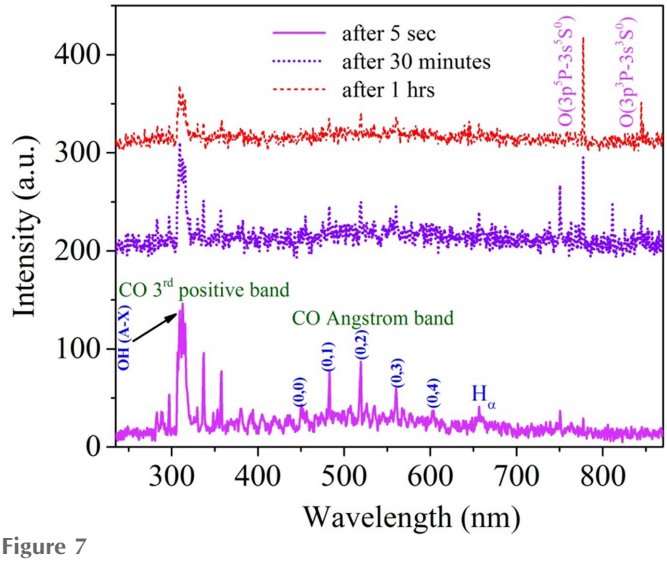

Figure 7
The optical emission spectrum of RF plasma irradiation of the toroidal mirror at the beginning (5 s), after 30 min and after 1 h. The image shows the spectrum recorded for the wavelength range of 250 to 900 nm.

Fig. 7 represents the intensity of the emission spectrum during RF plasma irradiation in the wavelength range of 250 to 900 nm, which contains both the ångström and third positive band of CO. The reduction in intensity of the vibrational transition of the second and third positive molecular bands shows a reduction in the density of CO molecules from the plasma volume with increasing RF irradiation time. This shows that the carbon layer starts to be removed from the surface of the mirror just after turning on the RF glow discharge.

We simultaneously observed the intensities of two lines of oxygen atomic transitions O ($3p^5P \rightarrow 3s^5S$) and O ($3p^3P \rightarrow 3s^3S$) at ∼778 and ∼842 nm, respectively (see Fig. 7). The intensities of both these lines increase with increasing irradiation time. This shows that there is an increase in the concentration of oxygen atoms in the glow discharge plasma, which indirectly confirms the reduction in carbon oxides.

Fig. 7 shows spectra for the plasma discharge just after switching on the process and later on, after 30 min and after 1 h of RF irradiation. It can be inferred from Fig. 7 that the line intensities of both bands of CO have been reduced almost to the level of noise due to complete removal of the carbon contamination layer after 1 h of RF plasma irradiation. Similar behaviour of decreasing intensities of the CO third positive band and ångström band and increasing intensity of oxygen atomic transitions during 50 to 140 s of exposure of a polyethylene terephthalate (PET) film by inductively coupled RF plasma were observed by Krstulović *et al.* (2006).

4. Summary

The removal of a carbon contamination layer from optical surfaces is a challenging task. Here, we have successfully removed the carbon contamination layer from a toroidal mirror (340 × 60 × 40 mm) using a capacitively coupled RF plasma method developed in-house, with Ar and O_2 as feedstock gases in a ratio of 1:1. Before cleaning the actual mirror, the RF power, exposure time and gas pressure were optimized using carbon-coated Pt samples [Si substrate/Pt (450 Å)/C (300 Å)]. The contaminated mirror was exposed to RF plasma for approximately 1 h under the pre-optimized conditions. To avoid surface damage by ion sputtering and to achieve uniformity in cleanness, the optical surface to be cleaned is mounted in the vertical direction.

The optical emission lines of CO and O from the plasma were monitored during the cleaning process, and a decreasing trend in CO optical band intensity and an increasing trend in O optical band intensity were observed. Before and after plasma exposure, the mirror was characterized by Raman spectroscopy, SXR and AFM techniques. The disappearance of the G and D bands of graphitic carbon in the Raman spectra after cleaning indicates the absence of a carbon layer. Moreover, the disappearance of the dip near the carbon

critical momentum transfer also shows the absence of a carbon layer.

Analysis of the SXR patterns also leads to the conclusion that the surface roughness of the Au layer remains the same before and after RF plasma cleaning. On the other hand, AFM images show that the surface morphology changes, with the surface roughness decreasing from 28 to 24 Å. The SXR in the energy range 750 to 1500 eV improved significantly.

Finally, we conclude that this toroidal mirror, that had become contaminated with carbon deposition in a synchrotron radiation beamline, was effectively cleaned using our RF plasma cleaning technique. The mirror's performance was retained after the plasma cleaning process, as confirmed from the energy-dependent SXR measurements.

Acknowledgements

The authors are grateful to Dr H. S. Patel and Dr M. K. Swami for providing the facility of Raman scattering measurements and for fruitful discussion. The authors are also grateful to Mr P. N. Rao and Mr P. D. Saxena for the AFM measurements and for support with the SXR measurements, respectively.

References

Attwood, D. (1999). *Soft X-rays and Extreme Ultraviolet Radiation: Principles and Applications*. New York: Cambridge University Press.

Belkind, A. & Gershman, S. (2008). *Plasma Cleaning of Surfaces*. *Vacuum Technology and Coatings*, pp. 46–57. Shenzhen: Jinghong Vacuum Thin Film.

Berman, D. & Krim, J. (2012). *Thin Solid Films*, **520**, 6201–6206.

Boller, K., Haelbich, R. P., Hogrefe, H., Jark, W. & Kunz, C. (1983). *Nucl. Instrum. Methods Phys. Res.* **208**, 273–279.

Chauvet, C., Polack, F., Silly, M. G., Lagarde, B., Thomasset, M., Kubsky, S., Duval, J. P., Risterucci, P., Pilette, B., Yao, I., Bergeard, N. & Sirotti, F. (2011). *J. Synchrotron Rad.* **18**, 761–764.

Chou, W.-C., Rex, C.-C., Wang, C.-L., Yang, C.-Y. & Lee, T.-M. (2017). *Materials*, **10**, 1223.

Cuxart, M., Reyes-Herrera, J., Šics, I., Goñi, A. R., Fernandez, H. M., Carlino, V. & Pellegrin, E. (2016). *Appl. Surf. Sci.* **362**, 448–458.

Dolgov, A., Lopaev, D., Lee, C. J., Zoethout, E., Medvedev, V., Yakushev, O. & Bijkerk, F. (2015). *Appl. Surf. Sci.* **353**, 708–713.

Graham, S., Steinhaus, C., Clift, M. & Klebanoff, L. (2002). *J. Vac. Sci. Technol. B*, **20**, 2393.

Henke, B. L., Gullikson, E. M. & Davis, J. C. (1993). *At. Data Nucl. Data Tables*, **54**, 181–342.

Hollenshead, J. & Klebanoff, L. (2006). *J. Vac. Sci. Technol. B*, **24**, 64–82.

Kim, M. C., Yang, S. H., Boo, J. H. & Han, J. G. (2003). *Surf. Coat. Technol.* **174–175**, 839–844.

Koide, T., Sato, S., Shidara, T., Niwano, M., Yanagihara, M., Yamada, A., Fujimori, A., Mikuni, A., Kato, H. & Miyahara, T. (1986). *Nucl. Instrum. Methods Phys. Res. A*, **246**, 215–218.

Koide, T., Shidara, T., Yanagihara, M. & Sato, S. (1988). *Appl. Opt.* **27**, 4305–4313.

Koide, T., Yanagihara, M., Aiura, Y., Sato, S., Shidara, T., Fujimori, A., Fukutani, H., Niwano, M. & Kato, H. (1987). *Appl. Opt.* **26**, 3884–3894.

Krstulović, N., Labazan, I., Milošević, S., Cvelbar, U., Vesel, A. & Mozetič, M. (2006). *J. Phys. D Appl. Phys.* **39**, 3799–3804.

Leontowich, A. F. G. & Hitchcock, A. P. (2012). *J. Vac. Sci. Technol. B*, **30**, 030601.

McKinney, W. R. & Takacs, P. Z. (1982). *Nucl. Instrum. Methods Phys. Res.* **195**, 371–374.

Modi, M. H., Gupta, R. K., Kane, S. R., Prasad, V., Garg, C. K., Yadav, P., Raghuvanshi, V. K., Singh, A. & Sinha, M. (2019). *AIP Conf. Proc.* **2054**, 060022.

Modi, M. H., Lodha, G. S., Mercere, P. & Idir, M. (2008). *Presented at the 9th International Conference on the Physics of X-ray Multilayer Structures*, 3–7 February 2008, Big Sky Resort, Montana, USA.

Moreno Fernández, H., Rogler, D., Sauthier, G., Thomasset, M., Dietsch, R., Carlino, V. & Pellegrin, E. (2018). *Sci. Rep.* **8**, 1293.

Nandedkar, R. V., Sawhney, K. J. S., Lodha, G. S., Verma, A., Raghuvanshi, V. K., Sinha, A. K., Modi, M. H. & Nayak, M. (2002). *Curr. Sci.* **82**, 298–304.

Parratt, L. G. (1954). *Phys. Rev.* **95**, 359–369.

Pellegrin, E., Šics, I., Reyes-Herrera, J., Perez Sempere, C., Lopez Alcolea, J. J., Langlois, M., Fernandez Rodriguez, J. & Carlino, V. (2014). *J. Synchrotron Rad.* **21**, 300–314.

Tuinstra, F. & Koenig, J. L. (1970). *J. Chem. Phys.* **53**, 1126–1130.

Wang, Y., Zhou, L., Jia, B., Bai, D., Yang, X., Gao, X. & Bo, B. (2012). *Proceedings of the International Conference on Optoelectronics and Microelectronics (ICOM)*, 23–25 August 2012, Changchun, Jilin, China, pp. 16–20.

Yadav, P. K., Gupta, R. K., Swami, M. K. & Modi, M. H. (2017). *J. Synchrotron Rad.* **24**, 757–764.

Yadav, P. K., Modi, M. H., Swami, M. K. & Singh, P. J. (2016). *J. Electron Spectrosc. Relat. Phenom.* **211**, 64–69.